Available online at www.sciencedirect.com
ScienceDirect
International Journal of Thermal Sciences 48 (2009) 353–362
International Journal of Thermal Sciences
www.elsevier.com/locate/ijts

Thermal and hydrodynamic analysis of gaseous flow in trapezoidal silicon microchannels

Lütfullah Kuddusi *, Edvin Çetegen

Istanbul Technical University, Faculty of Mechanical Engineering, Mechanical Engineering Department, Gümüşsuyu, 34437 Istanbul, Turkey

Received 8 May 2006; received in revised form 5 July 2007; accepted 24 February 2008

Available online 18 March 2008

Abstract

Thermal and hydrodynamic character of a hydrodynamically developed and thermally developing flow in trapezoidal silicon microchannels is analyzed. The continuum momentum and energy equations, with the velocity slip and temperature jump condition at the solid walls, are solved numerically in a square computational domain obtained by transformation of the trapezoidal geometry. The effects of rarefaction, aspect ratio and a parameter representing the fluid/wall interaction on thermal and hydrodynamic character of flow in trapezoidal microchannels are explored. It is found that the friction factor decreases if rarefaction and/or aspect ratio increase. It is also found that at low rarefactions the very high heat transfer rate at the entrance diminishes rapidly as the thermally developing flow approaches fully developed flow. At high rarefactions, heat transfer rate does not exhibit considerable changes along the microchannel, no matter the flow is developing or not.
© 2008 Elsevier Masson SAS. All rights reserved.

Keywords: Microchannel; Trapezoidal; Silicon; Heat transfer; Friction factor; Slip flow; Nusselt number

1. Introduction

A clear understanding of hydrodynamic and thermal behavior of gaseous flows in microchannels has become a requirement as the micro-fluidic applications grow rapidly. The hydrodynamic and thermal characteristics of flow in microtubes have been widely studied [1–5]. The one-dimensional character of flow in microtubes makes the analysis simpler relative to the flow in microchannels of non-circular shape, which requires a two-dimensional analysis. The practically used microchannels with non-circular cross section are those with rectangular, trapezoidal and hexagonal (double trapezoidal) cross section shapes. The shape of cross section is a result of microchannel production technology. Morini et al. [6] describe the chemical etching that is the most commonly used technique for building microchannels on silicon wafers. The microchannels produced by chemical etching directly on the silicon wafers have a cross-sectional shape that depends on a variety of factors such as the crystallographic nature of the silicon used. When a photolithographic process is employed, one can produce microchannels with a cross-section fixed by the orientation of the silicon crystal planes; for example, the microchannels etched in ⟨100⟩ and in ⟨110⟩ silicon using a KOH solution have a trapezoidal cross section (with an apex angle of 54.74° imposed by the crystallographic morphology of the ⟨100⟩ silicon) and a rectangular cross section, respectively.

In the past decade, a number of experimental and analytical works have conducted rectangular microchannel flows [7–10]. However, literature is still poor regarding trapezoidal and hexagonal microchannel flows. A summary of studies on single phase flow, liquid or gas, in trapezoidal microchannels is given below. The works dealing with single phase liquid flow in trapezoidal microchannels is given first.

Wu and Cheng [11] measured, experimentally, the friction factor of laminar flow of deionized water in smooth silicon microchannels of trapezoidal cross-section. It is shown that the friction constant of these microchannels is greatly influenced by the cross-sectional aspect ratio. Wu and Cheng [11] give a correlation equation for the friction constant of a fully developed laminar flow of water in these microchannels in terms of the cross-sectional aspect ratio.

* Corresponding author. Tel.: +90 212 2931300 (2452); fax: +90 212 2450795.
E-mail addresses: kuddusi@itu.edu.tr (L. Kuddusi), cetegenedv@itu.edu.tr (E. Çetegen).

1290-0729/$ – see front matter © 2008 Elsevier Masson SAS. All rights reserved.
doi:10.1016/j.ijthermalsci.2008.02.004

Nomenclature

a	non-dimensional long base of microchannel
a_i	long base of microchannel
A_c	cross sectional area
$A_{c,\xi\eta}$	non-dimensional cross sectional area
b	non-dimensional short base of microchannel
b_i	short base of microchannel
c_P	specific heat
D_h	hydraulic diameter ($4A_c/\Gamma_i$)
f	fanning friction factor
F_t	thermal accommodation coefficient
F_v	tangential momentum accommodation coefficient
h	convective heat transfer coefficient
h	non-dimensional height of microchannel
h_i	height of microchannel
k	thermal conductivity
Kn	Knudsen number
ℓ_h	heated perimeter of microchannel
L_h	non-dimensional heated perimeter of microchannel
n_i	normal to the inside boundaries
n	normal to the non-dimensional inside boundaries
Nu	Nusselt number
Nu_∞	fully developed Nusselt number
p	fluid pressure
P	normalized pressure gradient
Pr	Prandtl number
q	heat flux
R	specific heat ratio
Re	Reynolds number
T	non-dimensional temperature
u	non-dimensional fluid velocity
w	fluid velocity
x, y, z	transformed coordinates
X, Y, Z	Cartesian coordinates

Greek symbols

α	thermal diffusivity
α	apex angle
β	non-dimensional variable defined by Eq. (30)
β_t	non-dimensional variable defined by Eq. (4)
β_v	non-dimensional variable defined by Eq. (3)
γ	aspect ratio
Γ_i	Inside periphery of microchannel
Γ	non-dimensional inside periphery of microchannel
λ_{mfp}	molecular mean free path
μ	dynamic viscosity
θ	temperature
ξ, η, ζ	non-dimensional coordinates

Subscripts

b	bulk property
m	mean value
s	fluid property near the wall
w	wall value
0	inlet property

Weilin et al. [12] investigated flow characteristics of water through trapezoidal silicon microchannels experimentally. Experimental results of Weilin et al. [12] show that pressure gradient and flow friction in microchannels are higher than those given by the conventional laminar flow theory. They claim that the measured higher pressure gradient and flow friction may be due to the effect of surface roughness of the microchannels.

Weilin et al. [13] investigated also heat transfer characteristics of water flowing through trapezoidal silicon microchannels experimentally, with a numerical analysis extension. They found that the experimentally determined Nusselt number is much lower than that given by the numerical analysis. They claim that the measured lower Nusselt numbers may be due to the effects of surface roughness of the microchannel walls. They propose a roughness-viscosity model to interpret the experimental data.

Wu and Cheng [14] have performed experiments to investigate the laminar convective heat transfer and pressure drop of water in trapezoidal silicon microchannels. It is found that the values of Nusselt number and apparent friction constant depend greatly on different geometric parameters. The laminar Nusselt number and apparent friction constant increase with the increase of surface roughness and surface hydrophilic property. Wu and Ping Cheng [14] give dimensionless correlations for the Nusselt number and the apparent friction constant for the flow of water in trapezoidal microchannels having different geometric parameters, surface roughnesses and surface hydrophilic properties.

Morini [15] carried out a work that deals with the analysis of fully developed laminar liquid flow through silicon microchannels with trapezoidal and double-trapezoidal cross sections. The hydrodynamic flow parameters, including friction factor, are evaluated numerically and given in the form of polynomial functions, useful for a first evaluation of these parameters instead of or before a CFD simulation approach.

Gas flow studies in trapezoidal silicon microchannels are fairly rare.

Ding et al. [16] have conducted experiments to investigate nitrogen gas flow characteristics through trapezoidal silicon microchannels. They found that the friction coefficient is no longer a constant, which is different from the conventional theory.

Morini et al. [6] studied the rarefaction and cross-section geometry effects on the friction factor of an incompressible gasous flow in silicon microchannels having a rectangular, trapezoidal and double-trapezoidal cross section. It is found that for the trapezoidal and double-trapezoidal microchannels, the influence of the aspect ratio on the friction factor is strong only if the aspect ratio is less than 0.5.

The summary above shows that the hydrodynamic and thermal aspects of liquid flow in trapezoidal microchannels have

already been studied. But, there exist only a few studies on hydrodynamic aspect of gaseous flow in trapezoidal microchannels and, nothing on thermal aspect. The present work is an attempt to fill the literature gap in this regard. The paper analyzes both the hydrodynamic and thermal aspects of a gaseous flow in the trapezoidal microchannels, with emphasis on the latter.

2. Slip flow effects in microchannel

A gaseous flow at low pressure or in a very small passage does not obey the classical continuum physics. Contrary to the fluid flow in continuum physics, such a flow exhibits a nonzero flow velocity at solid boundaries and a nonzero difference between temperatures of solid boundaries and flow near solid boundaries. In other words, a slip flow and a temperature jump (non-equilibrium thermodynamics) will be present at solid boundaries, which are major effects of rarefaction and change in the physics of flow.

Consider a hydrodynamically developed and thermally developing steady flow in a trapezoidal microchannel. If the flow pressure is low, or, the microchannel sizes are very small, which is supposed to be the case in this paper, a slip flow occurs. Different from non-slip flow, the flow velocity is no longer zero at microchannel walls under slip flow. A molecular flow with nonzero velocity at microchannel boundaries occurs. Apart from nonzero flow velocity at the boundaries, a nonzero difference between the temperatures of the boundaries and the flow near the boundaries occurs as well. The local velocity and temperature of the flow near the walls for slip flow are given by Barron et al. [5], as

$$w_s = \beta_v \lambda_{\mathrm{mfp}} \left.\frac{\partial w}{\partial n_i}\right|_{\Gamma_i} \tag{1}$$

$$\theta_s = \theta_w + \beta_t \lambda_{\mathrm{mfp}} \left.\frac{\partial \theta}{\partial n_i}\right|_{\Gamma_i} \tag{2}$$

where n_i and Γ_i denote the normal to the inside boundaries and inside periphery of the microchannel, respectively, and the parameters β_v and β_t are given as

$$\beta_v = \frac{2 - F_v}{F_v} \tag{3}$$

$$\beta_t = \frac{2 - F_t}{F_t} \frac{2R}{1+R} \frac{1}{Pr} \tag{4}$$

The coefficients F_v and F_t are tangential momentum accommodation coefficient and thermal accommodation coefficient, respectively. For real walls some molecules reflect diffusively and some reflect specularly. These coefficients are defined as the fraction of molecules reflected diffusively [17]. Depending on the fluid, the solid and the surface finish these coefficients vary from 0 to 1.

The effect of rarefaction on flow properties is quantified by introducing the Knudsen number, which is defined as the ratio of the mean free molecular path to the characteristic length of flow field. The Knudsen number equal to zero corresponds to non-slip flow with zero flow velocity and zero difference between the temperatures of the boundaries and adjacent flow. As the Knudsen number takes a nonzero value, a slip flow with nonzero flow velocity at the boundaries and nonzero temperature difference between the boundaries and adjacent flow takes place. The higher Knudsen number causes higher rarefaction effects, namely, higher flow velocity and temperature jump at the boundaries. Beskok and Karniadakis [18] give the classification to differentiate the flow types. In this paper the concentration is on the slip flow with the Knudsen number ranging from 0.001 to 0.1. The Knudsen number in trapezoidal microchannel is defined as the ratio of the mean free molecular path to the hydraulic diameter. Therefore, with the mean free molecular path of gaseous medium at atmospheric conditions being about 0.1 μm [6], the given range for the Knudsen number limits the scope of the study to trapezoidal microchannels with hydraulic diameters ranging from 1 to 100 μm. Such microchannels may be used in cooling of microelectronic devices.

The study in this paper is limited to incompressible flows. According to Li et al. [19] the flow can be considered incompressible for Mach numbers lower than 0.3. In order to obtain the upper limit of Reynolds number for which the flow is incompressible, Morini et al. [6] give the following equation that relates Reynolds number, Mach number and Knudsen number in microchannel flow.

$$Re = \frac{Ma}{Kn}\sqrt{\frac{\pi R}{2}} \tag{5}$$

Keeping Mach number fixed at 0.3, this relation provides a possibility to determine the upper limit of Reynolds number for which the flow can be considered incompressible for a given Knudsen number. For example, the air flow in a microchannel can be considered incompressible, for Reynolds number as low as $Re < 4.45$ at upper limit of slip flow ($Kn = 0.1$), and for $Re < 445$ at lower limit of slip flow ($Kn = 0.001$). The results of the present study is valid for incompressible flow for which the upper limits of Mach number and Reynolds number are obtained as explained above.

3. Governing equations and modified boundary conditions

The flow is governed by the Navier–Stokes equations if the continuum condition (very low Knudsen number, $Kn < 10^{-3}$) is satisfied. The continuum form of flow does not exist in a microchannel under slip flow. Therefore the slip flow solution by using the Navier–Stokes equations may result in no negligible deviations in the hydrodynamic and thermal properties of the flow. However, the general belief of the investigators is that the Navier–Stokes equations may be used for slip flow solution with high accuracy provided the boundary conditions are modified according to the slip flow characteristics. Modification of the boundary conditions (nonzero flow velocity and temperature jump at the boundaries) removes the error raised by not properly using the Navier–Stokes equations in slip flow solution.

3.1. Momentum equation

The geometry of trapezoidal microchannel is shown in Fig. 1. The apex angle is equal to 54.74°, which is dictated

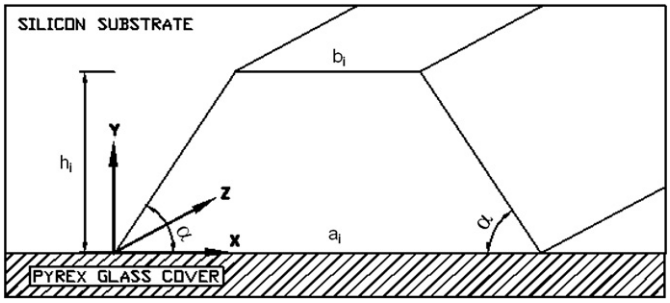

Fig. 1. The original geometry of trapezoidal silicon microchannel.

by silicon based microchannel manufacturing technology. The momentum equation for an incompressible viscous flow in the trapezoidal microchannel at steady state and hydrodynamically developed condition is given as

$$\frac{\partial^2 w}{\partial X^2} + \frac{\partial^2 w}{\partial Y^2} = \frac{1}{\mu}\frac{dp}{dZ} \tag{6}$$

The momentum equation will be non-dimensionalized by implementation of the following non-dimensional terms,

$$\xi = \frac{X}{D_h} \tag{7}$$

$$\eta = \frac{Y}{D_h} \tag{8}$$

$$\zeta = \frac{Z}{D_h}\frac{\alpha}{P w_m D_h} \tag{9}$$

$$u = \frac{w}{w_m P} \tag{10}$$

where the fluid mean velocity w_m and the normalized pressure gradient P are defined, respectively, as

$$w_m = \frac{1}{A_c}\int_{A_c} w(X,Y)\,dA_c \tag{11}$$

$$P = \frac{D_h^2}{w_m \mu}\frac{\partial p}{\partial Z} \tag{12}$$

A_c denotes the cross sectional area. The non-dimensional momentum equation is found as

$$\frac{\partial^2 u}{\partial \xi^2} + \frac{\partial^2 u}{\partial \eta^2} = 1 \tag{13}$$

The modified hydrodynamic boundary condition, Eq. (1), is also non-dimensionalized as

$$u_s = \beta_v Kn \left.\frac{\partial u}{\partial n}\right|_{\Gamma} \tag{14}$$

where the Knudsen number Kn is defined as

$$Kn = \frac{\lambda_{\mathrm{mfp}}}{D_h} \tag{15}$$

3.2. Energy equation

The energy equation for an incompressible viscous flow with negligible axial heat conduction in the trapezoidal microchannel at steady state and thermally developing condition is given as

$$\frac{\partial^2 \theta}{\partial X^2} + \frac{\partial^2 \theta}{\partial Y^2} = \frac{w}{\alpha}\frac{\partial \theta}{\partial Z} \tag{16}$$

The microchannel is heated from the top and the two side walls with a constant heat flux q. The bottom wall is covered by a Pyrex glass and is assumed to be adiabatic. The thermal boundary conditions of flow are given as

$$\left.\frac{\partial \theta}{\partial Y}\right|_{Y=0} = 0 \tag{17}$$

$$k\left.\frac{\partial \theta}{\partial Y}\right|_{Y=h_i} = q \tag{18}$$

$$-k\left.\frac{\partial \theta}{\partial n_i}\right|_{\mathrm{LeftWall}} = q \tag{19}$$

$$-k\left.\frac{\partial \theta}{\partial n_i}\right|_{\mathrm{RightWall}} = q \tag{20}$$

$$\theta|_{Z=0} = \theta_0 \tag{21}$$

The energy equation and thermal boundary conditions will be non-dimensionalized by implementation of the same non-dimensional terms used for the momentum equation and,

$$T = \frac{\theta - \theta_0}{(q D_h/k)} \tag{22}$$

The non-dimensional energy equation and thermal boundary conditions are found as

$$\frac{\partial^2 T}{\partial \xi^2} + \frac{\partial^2 T}{\partial \eta^2} = u\frac{\partial T}{\partial \zeta} \tag{23}$$

$$\left.\frac{\partial T}{\partial \eta}\right|_{\eta=0} = 0 \tag{24}$$

$$\left.\frac{\partial T}{\partial \eta}\right|_{\eta=h} = 1 \tag{25}$$

$$-\left.\frac{\partial T}{\partial n}\right|_{L.W.} = 1 \tag{26}$$

$$-\left.\frac{\partial T}{\partial n}\right|_{R.W.} = 1 \tag{27}$$

$$T|_{\zeta=0} = 0 \tag{28}$$

The modified thermal boundary condition, Eq. (2), is also non-dimensionalized as

$$T_s = T_w + \beta\beta_v Kn \left.\frac{\partial T}{\partial n}\right|_{\Gamma} \tag{29}$$

where β is defined as [20],

$$\beta = \frac{\beta_t}{\beta_v} \tag{30}$$

4. Transformation of geometry

The momentum and energy equations with associated boundary conditions, the set of Eqs. (13)–(14) and Eqs. (23)–(29), are to be solved. Analytical solution of these equations in a

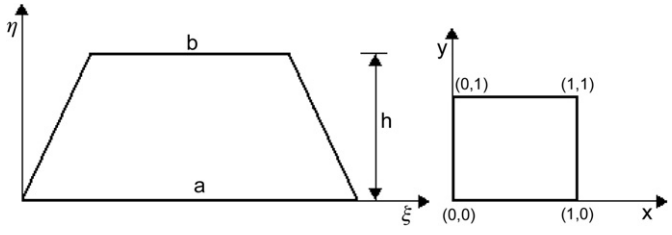

Fig. 2. The non-dimensional trapezoidal and transformed square geometries.

trapezoidal geometry is not possible. Therefore a numerical solution scheme will be applied. Application of a finite difference scheme in the trapezoidal geometry of microchannel is somehow difficult because of non-uniform mesh requirement on the left and right boundaries. Transformation of trapezoidal geometry to geometry with uniform grid generation possibility would simplify the application of finite difference scheme to the problem.

The following transformation [12] converts the trapezoidal geometry of the microchannel to a square with side length equal to unity. The non-dimensional trapezoidal and transformed geometries are shown in Fig. 2.

$$y = \frac{\eta}{h} \tag{31}$$

$$x = \frac{2h\xi - (a-b)\eta}{2ha - 2(a-b)\eta} \tag{32}$$

$$z = \zeta \tag{33}$$

Applying the transformation above to the momentum and energy equations (Eqs. (13) and (23)) leads to their transformed form, respectively, as

$$C_1\frac{\partial^2 u}{\partial y^2} + C_2\frac{\partial^2 u}{\partial x^2} + C_3\frac{\partial^2 u}{\partial y\partial x} + C_4\frac{\partial u}{\partial x} = 1 \tag{34}$$

$$C_1\frac{\partial^2 T}{\partial y^2} + C_2\frac{\partial^2 T}{\partial x^2} + C_3\frac{\partial^2 T}{\partial y\partial x} + C_4\frac{\partial T}{\partial x} = u(\xi,\eta)\frac{\partial T}{\partial z} \tag{35}$$

where,

$$C_1 = \frac{1}{h^2} \tag{36}$$

$$C_2 = \frac{(a-b)^2(2x-1)^2}{4h^2[a-(a-b)y]^2} + \frac{1}{[a-(a-b)y]^2} \tag{37}$$

$$C_3 = \frac{(a-b)(2x-1)}{h^2[a-(a-b)y]} \tag{38}$$

$$C_4 = \frac{(a-b)^2(2x-1)}{h^2[a-(a-b)y]^2} \tag{39}$$

The transformed forms of the hydrodynamic slip flow boundary condition (Eq. (14)) for the four microchannel walls are found as

$$u_s|_{y=0} = \beta_v Kn\left[\frac{(a-b)(2x-1)}{2ha}\frac{\partial u}{\partial x} + \frac{1}{h}\frac{\partial u}{\partial y}\right]_{y=0} \tag{40}$$

$$u_s|_{y=1} = -\beta_v Kn\left[\frac{(a-b)(2x-1)}{2hb}\frac{\partial u}{\partial x} + \frac{1}{h}\frac{\partial u}{\partial y}\right]_{y=1} \tag{41}$$

$$u_s|_{x=0} = \beta_v Kn\left[\frac{1}{[a-(a-b)y]\sin\alpha}\frac{\partial u}{\partial x} - \frac{\cos\alpha}{h}\frac{\partial u}{\partial y}\right]_{x=0} \tag{42}$$

$$u_s|_{x=1} = -\beta_v Kn\left[\frac{1}{[a-(a-b)y]\sin\alpha}\frac{\partial u}{\partial x} + \frac{\cos\alpha}{h}\frac{\partial u}{\partial y}\right]_{x=1} \tag{43}$$

The transformed forms of the thermal slip flow boundary condition (Eq. (29)) for the four microchannel walls are found as

$$T_s|_{y=0} = T_w|_{y=0} \tag{44}$$

$$T_s|_{y=1} = \left\{T_w - \beta\beta_v Kn\left[\frac{(a-b)(2x-1)}{2hb}\frac{\partial T}{\partial x} + \frac{1}{h}\frac{\partial T}{\partial y}\right]\right\}_{y=1} \tag{45}$$

$$T_s|_{x=0} = \left\{T_w + \beta\beta_v Kn\left[\frac{1}{[a-(a-b)y]\sin\alpha}\frac{\partial T}{\partial x} - \frac{\cos\alpha}{h}\frac{\partial T}{\partial y}\right]\right\}_{x=0} \tag{46}$$

$$T_s|_{x=1} = \left\{T_w - \beta\beta_v Kn\left[\frac{1}{[a-(a-b)y]\sin\alpha}\frac{\partial T}{\partial x} + \frac{\cos\alpha}{h}\frac{\partial T}{\partial y}\right]\right\}_{x=1} \tag{47}$$

The transformed forms of the thermal boundary conditions (Eqs. (24)–(28)) are also found, respectively, as

$$\left[\frac{(a-b)(2x-1)}{2ha}\frac{\partial T}{\partial x} + \frac{1}{h}\frac{\partial T}{\partial y}\right]_{y=0} = 0 \tag{48}$$

$$\left(\frac{(a-b)(2x-1)}{2hb}\frac{\partial T}{\partial x} + \frac{1}{h}\frac{\partial T}{\partial y}\right)_{y=1} = 1 \tag{49}$$

$$\frac{1}{[a-(a-b)y]\sin\alpha}\frac{\partial T}{\partial x}\bigg|_{x=0} - \frac{\cos\alpha}{h}\frac{\partial T}{\partial y}\bigg|_{x=0} = -1 \tag{50}$$

$$\frac{-1}{[a-(a-b)y]\sin\alpha}\frac{\partial T}{\partial x}\bigg|_{x=1} - \frac{\cos\alpha}{h}\frac{\partial T}{\partial y}\bigg|_{x=1} = -1 \tag{51}$$

$$T|_{z=0} = 0 \tag{52}$$

The set of Eqs. (34)–(52) will be solved numerically. Since the momentum equation is uncoupled with the energy equation, it will be solved first. The velocity field found by solution of the momentum equation will be used in the solution of energy equation in the next step.

Although the transformation above simplifies application of finite difference scheme by introducing a uniform grid generation possibility but, on the other hand, it rises the algebraic complexity of the set of equations to be solved. Compare the set of Eqs. (13)–(14) and Eqs. (23)–(29) with the set of Eqs. (34)–(52).

5. Numerical solution

A finite difference scheme is applied to solve the momentum and energy equations subject to the boundary conditions. A square mesh with $N \times N$ nodal points, including the boundary points, is used. The momentum and energy equations and all the boundary conditions are expressed in discrete form by applying a second order central difference scheme. Handling of boundary conditions at the boundary nodal points, especially at the corner points, requires an unusual treatment. In this study, imaginary grid points are located just before the boundary

points outside the computational region. This allowed applying the second order finite difference scheme to the boundary points as well, which in turn resulted in higher accuracy of the overall solution. The finite difference form of the momentum equation and the boundary conditions are written for the nodal points and the set of resulting $N \times N$ explicit linear equations is solved to find the velocity field first. Once the velocity field is known, one may have insight on hydrodynamic character of the flow in the microchannel by performing calculations on friction factor. The knowledge of velocity field allows solving the explicit finite difference form of the energy equation, subject to the boundary conditions, written for the nodal points to find the temperature field in the second step. The knowledge of velocity and temperature fields enables one to have insight on thermal character of the flow in the microchannel by performing calculations on the Nusselt number. Both the friction factor and Nusselt number that are the two major subject of studies in the microchannels are calculated for the trapezoidal microchannel at different geometrical conditions.

6. Calculations for friction factor and Nusselt number

The Poiseuille number fRe for a hydrodynamically developed laminar flow in the microchannel is calculated by [6],

$$fRe = -\frac{1}{2A_{c,\xi\eta}} \int_{\Gamma} \left.\frac{\partial u}{\partial n}\right|_{\Gamma} d\Gamma = \frac{P}{2} \tag{53}$$

where f represents the Fanning friction factor.

By non-dimensionalizing Eq. (11) one can find,

$$P = \frac{1}{u_m} \tag{54}$$

where u_m is the non-dimensional fluid bulk mean velocity calculated by

$$u_m = \frac{1}{A_{c,\xi\eta}} \int_{A_{c,\xi\eta}} u \, dA_{c,\xi\eta} \tag{55}$$

and where $A_{c,\xi\eta}$ represents the non-dimensional cross sectional area of the microchannel.

Combining Eq. (53) with Eq. (54) gives

$$fRe = \frac{1}{2u_m} \tag{56}$$

The local Nusselt number is calculated by

$$Nu(Z) = \frac{h(Z).D_h}{k} \tag{57}$$

An energy balance on the heated perimeter of a differential dZ segment at a specified Z-cross section of microchannel leads to

$$q.\ell_h \, dZ = h(Z).\ell_h \, dZ.\left[\theta_w(Z) - \theta_b(Z)\right] \tag{58}$$

where ℓ_h denotes the heated perimeter of the microchannel and the fluid bulk temperature θ_b is defined as

$$\theta_b(Z) = \frac{1}{A_c w_m} \int_{A_c} w(X,Y)\theta(X,Y) \, dA_c \tag{59}$$

The fluid bulk temperature may also be expressed in terms of non-dimensional variables as

$$T_b(Z) = \frac{1}{A_{c,\xi\eta} u_m} \int_{A_{c,\xi\eta}} uT \, dA_{c,\xi\eta} \tag{60}$$

The wall temperature $\theta_w(Z)$ is assumed to be equal to the sum of local wall temperatures averaged on the heated perimeter of the microchannel,

$$\theta_w(Z) = \frac{1}{\ell_h} \int_{\ell_h} \theta_w(X,Y) \, d\ell_h \tag{61}$$

This can also be non-dimensionalized to obtain the non-dimensional average wall temperature $T_w(Z)$ as

$$T_w(Z) = \frac{1}{L_h} \int_{L_h} T_w(\xi,\eta) \, dL_h \tag{62}$$

where L_h denotes the non-dimensional heated perimeter of the microchannel.

Combining Eq. (57) with Eq. (58) and using the non-dimensional wall and fluid bulk temperatures result in Nusselt number as

$$Nu(Z) = \frac{1}{T_w(Z) - T_b(Z)} \tag{63}$$

The integrals appearing in expressions for the non-dimensional wall and fluid bulk temperatures are approximated and calculated numerically.

7. Results and discussion

A computer program is developed to calculate the velocity field, local temperature field, friction factor and local Nusselt number along the thermally developing region of trapezoidal microchannel. The analysis shows that the velocity field, local temperature field, friction factor and local Nusselt number are functions of the aspect ratio γ, the parameter β and the rarefaction represented by $(\beta_v Kn)$. The effects of these parameters on hydrodynamic and thermal behavior of trapezoidal microchannel are studied. The aspect ratio is defined as $\gamma = h_i/a_i$ that varies from a maximum value of 0.707 (triangular microchannel) to a minimum value of zero (flat plate). The values in between correspond to trapezoidal microchannels. The group $(\beta_v Kn)$, representing the rarefaction effect, ranges from 0.001 to 0.1 in slip flow. The parameter β is a function of the thermal accommodation coefficient F_t, the tangential momentum accommodation coefficient F_v, the specific heat ratio R and the Prandtl number Pr. For most of engineering applications both the F_v and F_t can be taken equal to unity, which lead to $\beta \cong 1.667$ for $R = 1.4$ and $Pr = 0.7$ [20]. Theoretically, β may vary from zero to high values such as 100. The particular case when $\beta = 0$ implies that the velocity slip at the solid boundaries is taken into account but the temperature jump is not.

First, the solution method of the paper is validated by running the computer program for a microchannel with apex angle changed from 54.74° to 90°, which converts the trapezoidal geometry to a rectangular one. The fully developed Nusselt

Table 1
Fully developed Nusselt numbers for rectangular microchannel

Kn	$\gamma = 0.2$	$\gamma = 0.4$	$\gamma = 0.6$	$\gamma = 0.8$	$\gamma = 1$
	Nu	Nu	Nu	Nu	Nu
0.02	2.235	2.451	2.617	2.740	2.829
0.04	2.119	2.324	2.477	2.589	2.669
0.06	2.005	2.196	2.337	2.437	2.508
0.08	1.898	2.075	2.203	2.293	2.356
0.10	1.798	1.962	2.078	2.158	2.214

Table 2
Fully developed Nusselt numbers for rectangular microchannel obtained by Kuddusi and Çetegen [21]

Kn	$\gamma = 0.2$	$\gamma = 0.4$	$\gamma = 0.6$	$\gamma = 0.8$	$\gamma = 1$
	Nu	Nu	Nu	Nu	Nu
0.02	2.292	2.462	2.597	2.698	2.770
0.04	2.189	2.333	2.444	2.526	2.585
0.06	2.072	2.196	2.289	2.357	2.406
0.08	1.955	2.062	2.141	2.198	2.240
0.10	1.843	1.936	2.004	2.053	2.088

Table 3
Poiseuille numbers for slip flow in trapezoidal microchannel

		$\beta_v Kn$				
		0.020	0.040	0.060	0.080	0.100
γ	0.1	17.017	14.627	12.758	11.304	10.145
	0.3	13.251	11.565	10.220	9.152	8.281
	0.4	12.122	10.682	9.518	8.581	7.805
	0.5	11.815	10.434	9.315	8.416	7.674
	0.7	11.507	10.165	9.079	8.203	7.479

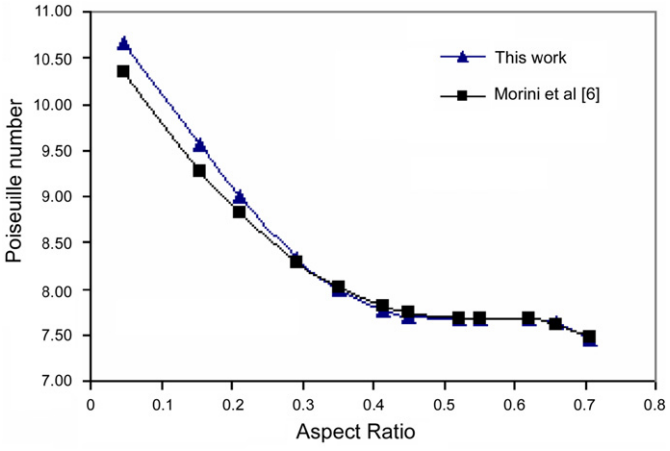

Fig. 3. Comparison of the Poiseuille numbers for slip flow in trapezoidal microchannel with those of Morini et al. [6] for the case $Kn = 0.1$.

Table 4
Comparison of Poiseuille numbers for continuum flow ($Kn = 0$) in trapezoidal microchannel with those (numerical and correlation) of Morini [15]

		Poiseuille numbers for continuum flow ($Kn = 0$)		
		Numerical results		Correlation
		This work	Morini [15]	Morini [15]
γ	0.047	21.952	22.174	22.144
	0.156	18.464	18.650	18.648
	0.211	17.072	17.244	17.236
	0.293	15.425	15.565	15.553
	0.414	13.950	14.063	14.053
	0.522	13.545	13.654	13.653
	0.707	13.202	13.308	13.306

numbers for such a rectangular microchannel are obtained and given in Table 1. The results agreed with those of Kuddusi and Çetegen [21], given in Table 2, who studied heat transfer in rectangular microchannels. Note that the results of Kuddusi and Çetegen [21] are for the 3S thermal version that corresponds to the three heated walls in this work. The results obtained for rectangular microchannel also agree well with the graphical results of Yu and Ameel [20]. The agreement between the results is an evidence of validity of the solution method employed in this paper.

In order to validate the solution method for trapezoidal microchannels too, the friction factor is calculated and compared with the results of Morini et al. [6] who investigated the friction factor in trapezoidal microchannel. The Poiseuille number that is a representative of friction factor is calculated as a function of aspect ratio γ and rarefaction represented by the group $\beta_v Kn$. The results are given on Table 3. Fig. 3 compares the Poiseuille numbers obtained in this work and those of Morini et al. [6] for the case $Kn = 0.1$. The comparison shows that the Poiseuille numbers obtained in this work agree well with those of Morini et al. [6].

The fully developed values of the Poiseuille numbers for continuum flow (no slip flow) are obtained by setting $\beta_v Kn$ equal to zero. Morini [15] also has given the fully developed values of the Poiseuille numbers for continuum liquid flow in trapezoidal microchannels by applying a numerical solution. Morini [15] has proposed also the following correlation for calculating the fully developed values of the Poiseuille numbers for continuum flow in trapezoidal microchannels.

$$fRe = 24 - 42.267\gamma + 64.272\gamma^2 - 118.42\gamma^3 + 242.12\gamma^4 - 178.79\gamma^5 \quad (64)$$

The fully developed values of the Poiseuille numbers for continuum flow obtained in this paper and those obtained by Morini [15] numerically and calculated using the correlation of Morini [15] are given in Table 4. The data on this table shows that the Poiseuille numbers obtained in this paper agree well with both the numerical results and correlation of Morini [15].

These validate the solution method, including the transformation of geometry and numerical scheme, applied for the momentum equation. Further, validation of the solution for momentum equation establishes an assurance for the accuracy of the solution for energy equation that employs the same transformation of geometry and numerical scheme.

The data on Table 3 shows that the rarefaction has a decreasing effect on the friction factor. The data also shows that the friction factor decreases if the aspect ratio increases, however, the rate of decrease in friction factor slows down for aspect ratios higher than 0.5.

It should be noted that the theoretically obtained data for friction factor disagree with the experimental data. Morini [22]

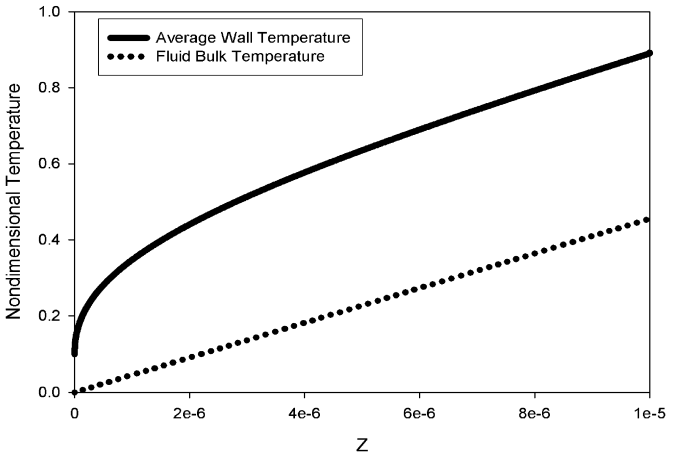

Fig. 4. Variation of non-dimensional wall and fluid bulk temperatures along a trapezoidal microchannel with $\beta \cong 1.667$ and $\gamma = 0.3$ at a rarefaction equal to $\beta_v Kn = 0.06$.

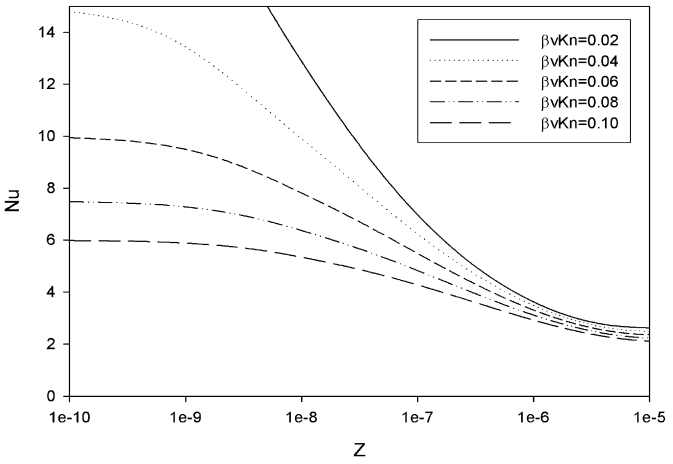

Fig. 5. Variation of local Nusselt number with rarefaction for thermally developing flow in a trapezoidal microchannel with $\beta \cong 1.667$ and $\gamma = 0.5$.

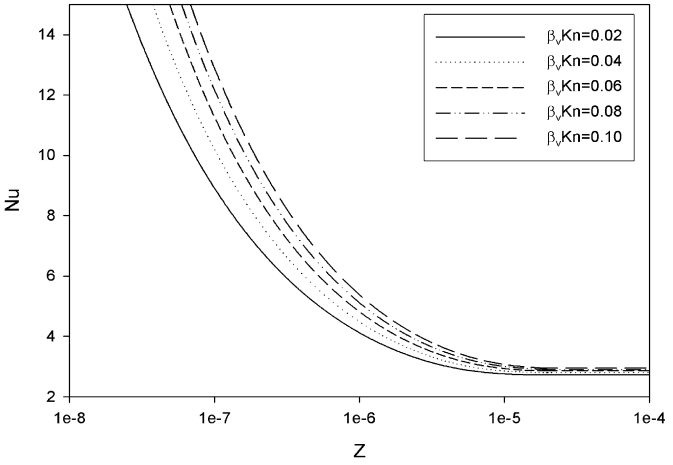

Fig. 6. Variation of local Nusselt number for a thermally developing flow in a trapezoidal microchannel with $\gamma = 0.3$ when the hydrodynamic effect of slip flow is present but the thermal effect is very weak ($\beta = 0.1$).

lists various reasons; rarefaction and compressibility effects, viscous dissipation effects, electro-osmotic effects (EDL), property variation effects, channel surface conditions (relative roughness) and experimental uncertainties, that account for the disagreement between theoretical and experimental data. The apex angle in trapezoidal microchannels also affects the friction factor.

Fig. 4 shows the typical variation of non-dimensional wall and fluid bulk temperatures along a trapezoidal microchannel with $\beta \cong 1.667$ and $\gamma = 0.3$ at a rarefaction equal to $\beta_v Kn = 0.06$. Since the three walls of the microchannel are subject to a constant heat flux, an increasing wall and fluid bulk temperatures along the microchannel is expected. The figure satisfies this expectation. The fluid enters the microchannel at a uniform temperature θ_0. This results in zero non-dimensional fluid bulk temperature at the entrance. If a non-slip flow ($\beta_v Kn = 0$) was considered, the non-dimensional wall temperature at the entrance would also be equal to zero. But, as Fig. 4 shows, a finite difference between the wall temperature and fluid bulk temperature at the entrance of the microchannel exists, which is the result of temperature jump at the solid walls caused by the slip flow in the microchannel. The finite difference between the wall temperature and fluid bulk temperature increases along the microchannel in the thermally developing flow region and reaches to a constant as the thermally developing flow approaches the fully developed flow. The small finite difference between the wall temperature and fluid bulk temperature is responsible for experiencing very high heat transfer rate (Nusselt number) at the entrance of the microchannel. The data found for the non-dimensional wall and fluid bulk temperatures agrees, qualitatively, with that of Yu and Ameel [20].

The effect of rarefaction on local Nusselt number for thermally developing flow in a trapezoidal microchannel with $\beta \cong 1.667$ and $\gamma = 0.5$ is shown in Fig. 5. As expected, very high heat transfer rates are experienced at low rarefactions in the entrance region of the microchannel. As expected also, high heat transfer rates at low rarefactions diminish rapidly as the thermally developing flow approaches the fully developed flow. Besides, high heat transfer rates in the entrance region of the microchannel lower intensely as the rarefaction increases. The figure shows that the difference between heat transfer rates for thermally developing and fully developed flows is not at considerable values at high rarefactions. In other words, overall heat transfer enhancement by high heat transfer rates in the entrance region for macrochannels is not experienced for microchannels, especially at high rarefactions.

Fig. 6 shows the variation of local Nusselt number for a thermally developing flow in a trapezoidal microchannel with $\gamma = 0.3$ when the hydrodynamic effect of slip flow is present but the thermal effect is very weak ($\beta = 0.1$). Eliminating the thermal effect of the slip flow, in other words, neglecting the temperature jump at solid boundaries results in extremely high heat transfer rates in the entrance region of the microchannel even at rarefactions as high as $\beta_v Kn = 0.10$. However, the heat transfer rate in the fully developed flow region of the microchannel lowers to the same order of magnitude as if the temperature jump at the solid boundaries is taken into account.

The effect of the parameter β is given in Fig. 7 in much diverse range. The figure shows the variation of local Nusselt

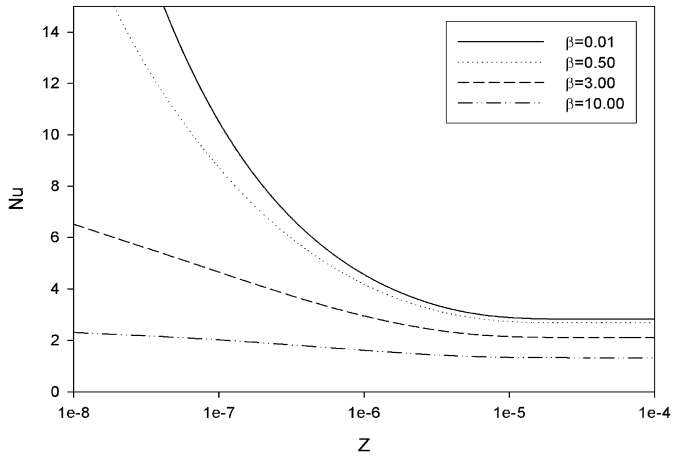

Fig. 7. Variation of local Nusselt number in the thermally developing flow region of a trapezoidal microchannel with $\gamma = 0.3$ and with $\beta_v Kn = 0.04$ for different values of the parameter β.

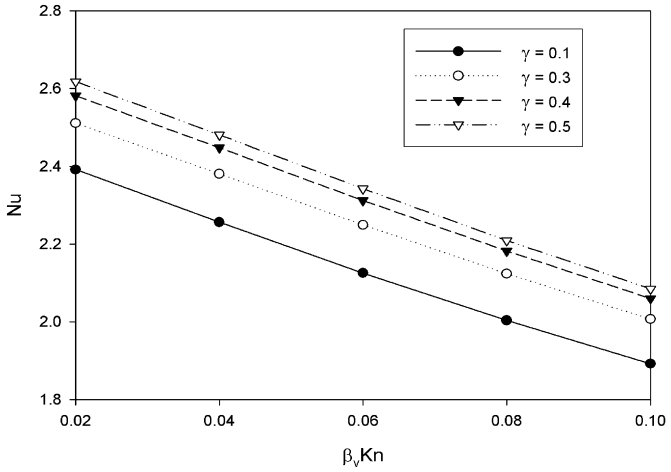

Fig. 8. Variation of Nusselt number (Nu_∞) in the fully developed flow region of a trapezoidal microchannel with $\beta \cong 1.667$.

number in the thermally developing flow region of a trapezoidal microchannel with $\gamma = 0.3$ and $\beta_v Kn = 0.04$ for different values of the parameter β. The heat transfer is high at the entrance but decreases rapidly along the microchannel in the thermally developing flow region for low values of the parameter β. In other words, in the presence of a slip flow in the microchannel with strong hydrodynamic but weak thermal effect, heat transfer decreases rapidly from a maximum at the entrance to a constant in the fully developed flow region. As discussed above, weakening the thermal effect of rarefaction lowers the value of temperature jump at the solid walls, which in turn causes to experience very high heat transfer rates especially at the entrance. However, for a slip flow in the microchannel with very strong thermal effect, the heat transfer rate does not exhibit a significant change along the microchannel. See the Nusselt number variation for $\beta = 10$ in Fig. 7.

Although this paper analyzes the thermally developing flow region, but it should not be forgotten that the contribution of this region, despite its very high heat transfer rate, on the overall heat transfer performance of the microchannel is extremely low, even negligible in long microchannels, due to short length of the thermally developing flow region. Therefore, from practical point of view, in order to evaluate the overall heat transfer performance of a microchannel it would be enough to evaluate its performance in the fully developed flow region. Fig. 8 shows the variation of Nusselt number (Nu_∞) in the fully developed flow region of a trapezoidal microchannel with $\beta \cong 1.667$. The decreasing effect of rarefaction on the fully developed Nusselt number (Nu_∞) is not surprising. The trapezoidal microchannel is heated from the two side and top walls. As the aspect ratio γ increases, the heated perimeter of the microchannel increases as well. At the limit ($\gamma = 0.707$), the trapezoidal microchannel changes to a triangular microchannel with the highest heated perimeter. One can expect higher heat transfer in a trapezoidal microchannel with higher heated perimeter (higher aspect ratio). Also, one can expect the highest heat transfer in a trapezoidal microchannel with the highest aspect ratio, namely in a triangular microchannel. The data in Fig. 8 is in conformity with these expectations.

8. Conclusion

Thermal and hydrodynamic character of a hydrodynamically developed and thermally developing flow in trapezoidal silicon microchannels is analyzed. The continuum approach with the velocity slip and temperature jump condition at the solid walls is applied to develop the mathematical model of flow phenomenon in the trapezoidal microchannel. A numerical approach to the problem is unavoidable because analytical solution of the developed mathematical model is not possible in the trapezoidal geometry. Therefore a finite difference scheme is preferred in solution of the problem. A transformation is applied to remove the difficulty raised by non-uniform mesh in the trapezoidal geometry. The transformation of trapezoidal geometry to a square provided ease of uniform mesh generating in the computational domain but, at the same time, increased the complexity of the mathematical model of the problem.

The solution method of the paper is validated twice. Since the developed computer program has the flexibility to simulate the flow in the trapezoidal microchannels with any given apex angle, first, the thermally developing and fully developed Nusselt numbers are calculated for a rectangular microchannel by changing the apex angle from 54.74° to 90°. The results agreed with those of Yu and Ameel [20] and Kuddusi and Çetegen [21] who studied heat transfer in rectangular microchannels. This is the first validation of the solution method. The agreement between the results of Morini et al. [6] and Morini [15] who investigated the friction factor in trapezoidal microchannels and those found in this paper validates the solution method for the second time. However, the results found for thermal character of flow are not validated because there exist no work in literature that deals with thermal character of gaseous flow in trapezoidal microchannels.

The paper explores the effects of rarefaction, aspect ratio and a parameter representing the fluid/wall interaction on thermal and hydrodynamic character of flow in trapezoidal microchan-

nels. It is found that the friction factor decreases if rarefaction and/or aspect ratio increase. It is also found that at low rarefactions the very high heat transfer rate at the entrance diminishes rapidly as the thermally developing flow approaches fully developed flow. At high rarefactions, heat transfer rate does not exhibit considerable changes along the microchannel, no matter the flow is thermally developing or not.

References

[1] G. Tunc, Y. Bayazitoglu, Heat transfer in microtubes with viscous dissipation, International Journal of Heat and Mass Transfer 44 (13) (2001) 2395–2403.
[2] S.M. Ghiaasiaan, T.S. Laker, Turbulent forced convection in microtubes, International Journal of Heat and Mass Transfer 44 (14) (2001) 2777–2782.
[3] H. Zhao, The numerical solution of gaseous slip flows in microtubes, International Communications in Heat and Mass Transfer 28 (4) (2001) 585–594.
[4] Z.Y. Guo, X.B. Wu, Compressibility effect on the gas flow and heat transfer in a microtube, International Journal of Heat and Mass Transfer 40 (13) (1997) 3251–3254.
[5] R.F. Barron, X. Wang, T.A. Ameel, R.O. Warrington, The Graetz problem extended to slip-flow, International Journal of Heat and Mass Transfer 40 (8) (1997) 1817–1823.
[6] G.L. Morini, M. Spiga, P. Tartarini, The rarefaction effect on the friction factor of gas flow in microchannels, Superlattices and Microstructures 35 (2004) 587–599.
[7] G. Tunc, Y. Bayazitoglu, Heat transfer in rectangular microchannels, International Journal of Heat and Mass Transfer 45 (4) (2002) 765–773.
[8] L. Ghodoossi, Eğrican, Prediction of heat transfer characteristics in rectangular microchannels for slip flow regime and H1 boundary condition, International Journal of Thermal Sciences 44 (6) (2005) 513–520.
[9] P.-S. Lee, S.V. Garimella, D. Liu, Investigation of heat transfer in rectangular microchannels, International Journal of Heat and Mass Transfer 48 (9) (2005) 1688–1704.
[10] T.M. Harms, M.J. Kazmierczak, F.M. Gerner, Developing convective heat transfer in deep rectangular microchannels, International Journal of Heat and Fluid Flow 20 (2) (1999) 149–157.
[11] H.Y. Wu, P. Cheng, Friction factors in smooth trapezoidal silicon microchannels with different aspect ratios, International Journal of Heat and Mass Transfer 46 (14) (2003) 2519–2525.
[12] W. Qu, G.M. Mala, D. Li, Pressure-driven water flows in trapezoidal silicon microchannels, International Journal of Heat and Mass Transfer 43 (3) (2000) 353–364.
[13] W. Qu, G.M. Mala, D. Li, Heat transfer for water flow in trapezoidal silicon microchannels, International Journal of Heat and Mass Transfer 43 (21) (2000) 3925–3936.
[14] H.Y. Wu, P. Cheng, An experimental study of convective heat transfer in silicon microchannels with different surface conditions, International Journal of Heat and Mass Transfer 46 (14) (2003) 2547–2556.
[15] G.L. Morini, Laminar liquid flow through silicon microchannels, Journal of Fluids Engineering, Transactions of the ASME 126 (3) (2004) 485–489.
[16] Y.-T. Ding, Z.-H. Yao, N.-Y. Shen, Gas flow characteristics in straight silicon microchannels, Chinese Physics 11 (9) (2002) 869–875.
[17] M. Gad-el-Hak, The MEMS Handbook, CRC Press LLC, Boca Raton, 2002.
[18] A. Beskok, G.E. Karniadakis, Simulation of slip-flows in complex microgeometries, in: ASME DSC, vol. 40, Micromechanical Systems. Book No. G00783-1992, 1992, pp. 355–370.
[19] Z.X. Li, D.X. Du, Z.Y. Guo, Characteristics of frictional resistance for gas flow in microtubes, in: Proc. Symposium on Energy Engineering in the 21st Century, vol. 2, 2000, pp. 658–664.
[20] S. Yu, T.A. Ameel, Slip-flow heat transfer in rectangular microchannels, International Journal of Heat and Mass Transfer 44 (22) (2001) 4225–4234.
[21] L. Kuddusi, E. Çetegen, Prediction of temperature distribution and Nusselt number in rectangular microchannels at wall slip condition for all versions of constant heat flux, International Journal of Heat and Fluid Flow 28 (4) (2007) 777–786.
[22] G.L. Morini, Single-phase convective heat transfer in microchannels: A review of experimental results, International Journal of Thermal Sciences 43 (7) (2004) 631–651.